

**EFFECTS OF ERRORS IN VELOCITY TILT ON MAXIMUM
LONGITUDINAL COMPRESSION DURING NEUTRALIZED DRIFT
COMPRESSION OF INTENSE BEAM PULSES: II. ANALYSIS OF
EXPERIMENTAL DATA OF THE NEUTRALIZED DRIFT COMPRESSION
EXPERIMENT- I (NDCX-I)**

Scott Massidda, Igor D. Kaganovich, Edward A. Startsev, and Ronald C. Davidson
Plasma Physics Laboratory, Princeton University, Princeton, NJ 08543

Steven M. Lidia, Peter Seidl,
Lawrence Berkeley National Laboratory, 1 Cyclotron Road, Berkeley, CA 94720

Alex Friedman
Lawrence Livermore National Laboratory, 7000 East Avenue, Livermore, CA 94550

Abstract

Neutralized drift compression offers an effective means for particle beam focusing and current amplification with applications to heavy ion fusion. In the Neutralized Drift Compression eXperiment-I (NDCX-I), a non-relativistic ion beam pulse is passed through an inductive bunching module that produces a longitudinal velocity modulation. Due to the applied velocity tilt, the beam pulse compresses during neutralized drift. The ion beam pulse can be compressed by a factor of more than 100; however, errors in the velocity modulation affect the compression ratio in complex ways. We have performed a study of how the longitudinal compression of a typical NDCX-I ion beam pulse is affected by the initial errors in the acquired velocity modulation. Without any voltage errors, an ideal compression is limited only by the initial thermal energy spread of the ion beam, ΔE_b . In the presence of large voltage errors, $\delta U \gg \Delta E_b$, the maximum compression ratio is found to be inversely proportional to the geometric mean of the relative error in velocity modulation and the relative intrinsic energy spread of the beam ions. Although small parts of a beam pulse can achieve high local values of compression ratio, the acquired velocity errors cause these parts to compress at different times, limiting the overall compression of the ion beam pulse.

18 I. INTRODUCTION

19

20 Longitudinal bunch compression is a standard technique used to increase the beam intensity in
21 various accelerators [1]. Previous longitudinal drift compression analysis has studied the effects of
22 intrinsic beam momentum spread, plasma, and solenoidal final focus conditions on compression [1,
23 2]. Much focus has also gone towards space-charge neutralization [1, 3]. The kinematics of
24 neutralized compression drift is well-developed [4]. Here, we focus on the most important effect
25 that limits the beam compression -- the errors in the voltage in the bunching module. This paper is
26 a companion paper of Ref. [5], which analyzes the general properties of the effects of errors on
27 longitudinal compression. Here, we apply the formalism developed in Ref. [5] to analysis of the
28 experimental data of the Neutralized Drift Compression eXperiment-I (NDCX-I).

29

30 In neutralized drift compression the applied velocity tilt, Δv_b , slows down the head of the ion beam
31 pulse and speeds up the tail of the pulse so that the entire beam pulse compresses at a later time, t_f ,
32 at the target plane, l_f . The velocity tilt is produced by an induction bunching module. Ideally, the
33 voltage profile of the induction bunching module is designed such that the entire beam pulse arrives
34 at one location at the focusing time. The corresponding beam velocity profile is called an ideal tilt.
35 In this case, the effects associated with a small thermal energy spread, ΔE_b would limit the
36 compression. For the NDCX-1 experiment the measurements of the thermal energy spread give
37 $\Delta E_b < 170 \text{ eV}$ [6]. However, voltage errors in the induction bunching module are of the order 1kV
38 and thus are primarily responsible for the limitation of longitudinal compression.

39

40 Due to voltage errors and corresponding errors in the applied velocity tilt, δv_b , parts of the ion beam
41 pulse arrive at different times. The compressed beam pulse width at the target chamber is of order
42 $l_f = \delta v_b t_f$, where t_f is the drift time. This gives a pulse duration of order $\delta v_b t_f / v_b^{in}$, where v_b^{in} is
43 the original velocity of the beam determined by the initial beam energy. During the drift, the head
44 and tail of the pulse of duration, t_p , approach the target nearly simultaneously, i.e., the pulse length
45 is $l_p \equiv v_b^{in} t_p = \Delta v_b t_f$. Correspondingly, the compression ratio is of order [5]

46

$$47 \quad C \sim \frac{l_p}{l_f} = \frac{v_b^{in} t_p}{\delta v_b t_f} = \frac{\Delta v_b}{\delta v_b}. \quad (1)$$

48 From Eq.(1), it is evident that the portion of the beam pulse with the smallest errors contributes
 49 most to the compression. If the velocity errors are much smaller for the fraction of the pulse, δt_p ,
 50 then the compression ratio is given by

$$51 \quad C \sim \frac{\Delta v_b \delta t_p}{\delta v_b t_p}. \quad (2)$$

52 If beam velocity errors become so small that they are comparable to the thermal spread, then the
 53 compression ratio is limited by the thermal velocity, v_T , i.e.,

$$54 \quad C \sim \frac{\Delta v_b \delta t_p}{v_T t_p}. \quad (3)$$

55 Correspondingly, the maximum compression ratio is determined by the condition when the largest
 56 fraction of the pulse compresses with the smallest velocity errors. For example, for a model of fast
 57 changing errors on a scale t_{er} that is small compared to the initial pulse width in the form,

$$58 \quad \delta v_b = \delta v_b \sin(t / t_{er}), \text{ the fraction of the pulse that compresses is given by } \delta t_p \approx t_{er} (4v_T / \delta v_b)^{1/2}$$

59 [5] and

$$60 \quad C \sim \frac{2\Delta v_b t_{er}}{(v_T \delta v_b)^{1/2} t_p}. \quad (4)$$

61 Therefore, the maximum compression ratio is a function of both the thermal spread and the velocity
 62 errors.

63

64 Using previously derived analytical formulas from Ref. [5] for calculating the compression ratio of
 65 a particular velocity tilt, together with particle-in-cell simulations, data from NDCX-I experiments
 66 have been analyzed using a fully kinetic treatment. It was found that the compression ratio is a
 67 function of both errors in the applied velocity tilt and the initial thermal energy spread of the beam
 68 pulse.

69

70 This paper is organized as follows: Section II provides the basic equations; Section III applies the
 71 results to the NDCX-I experiment; and Section IV summarizes the conclusions.

72

73 II. BASIC EQUATIONS

74

75 In this section we provide a summary of the analytical description of the longitudinal compression
 76 ratio, explained in greater detail in Ref. [5]. First, we describe the compression ratio without taking
 77 thermal effects into account. The beam acquires velocity, $v_b(\tau)$, in the induction bunching module,
 78 where τ denotes the time at which the beam interacts with the bunching module. The head of the
 79 pulse acquires velocity $v_{b0} \equiv v_b(0)$. The parameter τ can be viewed as a marker for a particular
 80 part of the ion beam pulse, $0 \leq \tau \leq t_p$, where t_p is the duration of the pulse that is expected to
 81 compress. The trajectory of a beam pulse at time t , interacting with the bunching module at time
 82 τ , is given by

$$83 \quad z_b(t, \tau) = v_b(\tau)(t - \tau), \quad (5)$$

84 which represents the acquired velocity multiplied by the drift time. An ideal trajectory has all parts
 85 of the beam pulse arriving at the target plane at the same time, $z_b(t_f, \tau) = l_f$, for all τ . This requires
 86 the *ideal* velocity tilt,

$$87 \quad v_b^i(\tau) = v_{b0} t_f / (t_f - \tau). \quad (6)$$

88 Note that $v_{b0} t_f = l_f$, and by varying the parameters v_{b0} and t_f , different ideal velocity tilts can be
 89 chosen that would allow the beam to compress at a certain location l_f or time t_f .

90

91 The longitudinal density is given by the ratio of the initial and final separation of the beam slices
 92 $n_b(\tau, t) = n_b^{in} |dz_0 / dz_b|$, where n_b^{in} is the initial beam ion line density before the bunching module.

93 Substituting for $z_b(t, \tau)$ from Eq. (5) gives

$$94 \quad n_b(\tau, t) = \frac{n_b^{in} v_b^{in}}{|v_b(\tau) - (t - \tau) dv_b(\tau) / d\tau|}. \quad (7)$$

95 A convenient way to characterize the compression of the pulse is to introduce the time to focus [5],
 96 $t_s(\tau)$, when different parts of the ion beam pulse compress, or when neighboring slices of the beam
 97 arrive at the same position. In Lagrangian coordinates, this corresponds to a singularity in the beam
 98 line density profile given by Eq.(7), which occurs at time

$$99 \quad t_s(\tau) = \frac{v_b(\tau)}{dv_b(\tau)/d\tau} + \tau. \quad (8)$$

100 An ideal velocity tilt will have $t_s(\tau) = t_f$ for all τ , which implies that all parts of the pulse
 101 compress at the same time.

102
 103 Another convenient way to examine the beam dynamics is by plotting the beam pulse in phase-
 104 space coordinates, (z, v_z) . As the beam moves through phase space, the velocity tilt that represents
 105 the beam moves with it, becoming a vertical line when the beam is compressed. Vertical lines in
 106 phase space correspond to peaks in compression. To remove the singularity in Eq. (7), the
 107 compression ratio has to be calculated by taking thermal effects into account. The compression ratio
 108 is determined by counting the number of particles that arrive at a certain location z , at time t [5],
 109 i.e.,

$$110 \quad n_b(z, t) = \int_{-\infty}^t v_b^{in} d\tau \int_{-\infty}^{\infty} dv f(v) \delta(z - z_b(t, \tau) - vt), \quad (9)$$

111 where $f(v)$ is the initial velocity distribution function of the beam ions. This formula allows the
 112 compression ratio to be calculated for any applied velocity tilt. The maximum compression ratio for
 113 an ideal tilt is obtained by comparing the initial pulse length, $t_p v_b^{in}$, to the final spread, limited only
 114 by the intrinsic Maxwellian velocity distribution of the initial pulse with mean velocity v_T [5], i.e.,

$$115 \quad C_{\max}^i = \frac{t_p v_b^{in}}{\sqrt{\pi} v_T t_f}. \quad (10)$$

116 For example, for NDCX-I parameters, the ion beam energy is 300keV, and $T_{bz} \simeq 0.3eV$,
 117 $v_T / v_b^{in} \approx 10^{-3}$; and for a velocity tilt, $\Delta v_b / v_b^{in} = t_p / t_f = 0.15$, $t_f \sim 3\mu s$, $t_p \sim 0.45\mu s$, and

118 Eq. (10) gives $t_f \sim 3\mu s$, $v_b t_p \sim 45cm$, $\sqrt{\pi}v_T t_f \sim 0.4cm$ and $C_{\max} = 110$. For the case of smaller
 119 $T_{bz} \simeq 0.05eV$, we obtain $C_{\max} = 255$.

120

121 This can be compared to the compression ratio of a pulse with voltage errors, δU . Here, the
 122 compression ratio is shown to be a weak function of thermal spread, v_T , and the relative error in
 123 applied energy $\delta U / E_b$ [5] is given by

$$124 \quad C_{\max}^b \approx \frac{\tau_\gamma}{t_f} \left(\frac{v_{b0}}{v_T \delta U / E_b} \right)^{1/2}. \quad (11)$$

125 Here, τ_γ is the characteristic temporal scale for a change in the velocity errors. For NDCX-I,

126 $\delta U / E_b \sim 1/300$, and $\tau_\gamma \sim 300ns$. This gives a maximum compression ratio of about 60.

127 Note that a thermal equilibrium distribution in beam energy corresponds to a Gaussian distribution
 128 in energy spread, $\Delta E_b \approx M(v - v_b)v_b$, with

$$129 \quad f_M(\Delta E) = \frac{1}{\sqrt{2\pi T_z / M}} \exp\left(-\frac{(\Delta E)^2}{4E_b T_z}\right).$$

130 Correspondingly, the standard deviation for the energy spread is $2\sqrt{E_b T_z}$; the average dispersion of

131 the energy spread is $\sqrt{\langle(\Delta E)^2\rangle} = \sqrt{2E_b T_z}$; and the full width at half maximum of the energy

132 spread is $2\sqrt{E_b T_z \ln(2)}$. For example, for $T_{bz} \simeq 0.1eV$ and $E_b = 300keV$, the energy spread

133 dispersion is 245eV and the standard deviation is 347eV.

134

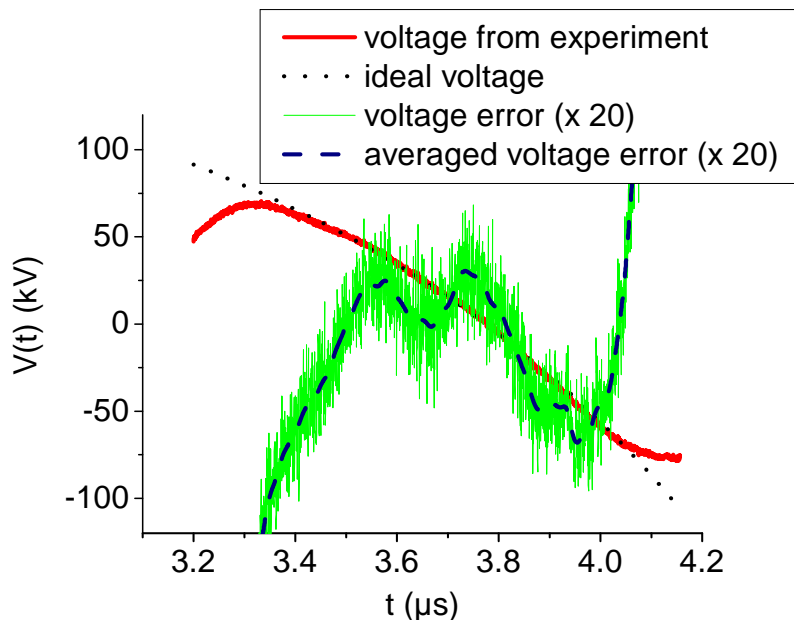
135 Based on the results of the experimental study in Ref. [7], the upper bound of the beam energy
 136 spread is 100eV (see Ref. [5] Section II c 2 for a more complete discussion). Consequently, it is
 137 assumed in the following analysis that $T_{bz} = T_i = 0.05 - 0.1eV$, and that the value is determined
 138 by the ion source temperature.

139

140 **III. ANALYSIS OF EFFECTS OF VOLTAGE ERRORS ON LONGITUDINAL**
 141 **COMPRESSION RATIO FOR NDCX-I EXPERIMENTS**

142

143 The NDCX-I experimental configuration is well described in several publications [8,9,10,11,12]. In
 144 these experiments, a potassium ion beam with energy of about 300keV passes through an induction
 145 bunching module and then drifts through a neutralized drift section of about 3 meters in length. As a
 146 result, part of the beam (about 500ns) is compressed to a few ns. Experimentally-achieved
 147 compression ratios range from 50 to 90, depending on the beam energy and the target location. We
 148 have performed a detailed analysis of the longitudinal compression ratio for the voltage pulse
 149 waveform shown in Fig. 1, and a drift section with length 286.8cm. The data is taken from Ref.
 150 [13]. We have found that the maximum compression ratio can increase from 60 to 90 for optimal
 151 beam energy, in agreement with the experimental data. We have also analyzed other data sets and
 152 found results similar to the data shown in Fig. 1.



153

154 Fig. 1. Plots of experimental voltage waveform of the NDCX-I induction bunching module [13] as a function of time
 155 and the ideal voltage waveform needed to compress the beam pulse at the target plane for beam energy 270keV (dotted
 156 curve). Also shown is the error in the experimental voltage as compared with the ideal voltage pulse and the Gaussian-
 157 weighted averaged value of the error with a 20ns time window performed to remove high-frequency noise.

158

159 As evident from Fig. 1, the experimental voltage waveform is close to the ideal voltage waveform
 160 pulse starting at $t_0 = 3.48\mu\text{s}$ and ending at $t_1 = 4.07\mu\text{s}$ for a total duration of $t_p = 0.59\mu\text{s}$. Therefore,

161 this part of the beam pulse is expected to compress. At the beginning of the pulse, the beam head is
 162 decelerated from 270kV to 210kV at $t_0 = 3.48\mu\text{s}$, and accelerated from 270kV to 348kV at the end
 163 of the pulse, at $t_1 = 4.07\mu\text{s}$. Note that the voltage polarity shown in Fig. 1 is such that a positive
 164 voltage corresponds to beam deceleration. The ideal voltage waveform is given by

$$165 \quad U(t) = \frac{M}{2} \left\{ \left[v_b^i(t) \right]^2 - v_b^2(t_0) \right\}, \quad (12)$$

166 where $v_b^i(\tau) = v_{b0} t_f / (t_f - \tau)$ and $\tau = (t - t_0)$. Here, we have assumed the thin-gap
 167 approximation, in which the drift time through the gap can be neglected. Corrections to the thin-gap
 168 approximation are discussed in the Ref. [5], and are mostly reduced to averaging the voltage errors

169 over the time scale of the drift through the gap, $V(\tau) \rightarrow \int_{-\infty}^{\infty} \frac{V(\tau')}{\Delta\tau\sqrt{\pi}} \exp\left[-\frac{(\tau' - \tau)^2}{\Delta\tau^2}\right] d\tau'$. The transit

170 time, $\Delta\tau$, is $b / v_b^{in} = 30\text{ns}$, where $b \approx 2 \times 0.73R_w / \sqrt{\pi}$ and R_w is the pipe radius [5].

171 *III.A Choosing parameters for an ideal voltage pulse*

172
 173 The applied voltage errors are at the level of several percent. Therefore, the ideal voltage waveform
 174 parameters (t_f and v_{b0} , or E_{b0} , the beam energy at the start of the beam pulse) can also be chosen
 175 within several percent accuracy, as evident in Fig. 2. For example, the choice of $t_f = 2.83\mu\text{s}$ and
 176 $E_{b0}=210\text{keV}$ corresponds to a beam pulse compressed at $v_{b0} t_f = 288.3\text{cm}$, in the limit of ideal
 177 compression ratio without any errors. This compression plane is slightly behind the target
 178 positioned at 286.8cm. Choosing $t_f = 2.679\mu\text{s}$ and $E_{b0}=217\text{keV}$ corresponds to the ideal beam
 179 pulse compressed at the target location, $v_{b0} t_f = 286.8\text{cm}$. Similarly, the choice of $t_f = 2.77\mu\text{s}$ and
 180 $E_{b0}=208\text{keV}$ corresponds to a compression plane located at $v_{b0} t_f = 281\text{cm}$, just before the target
 181 plane. The compressed beam profiles at different locations are shown in Fig. 3.

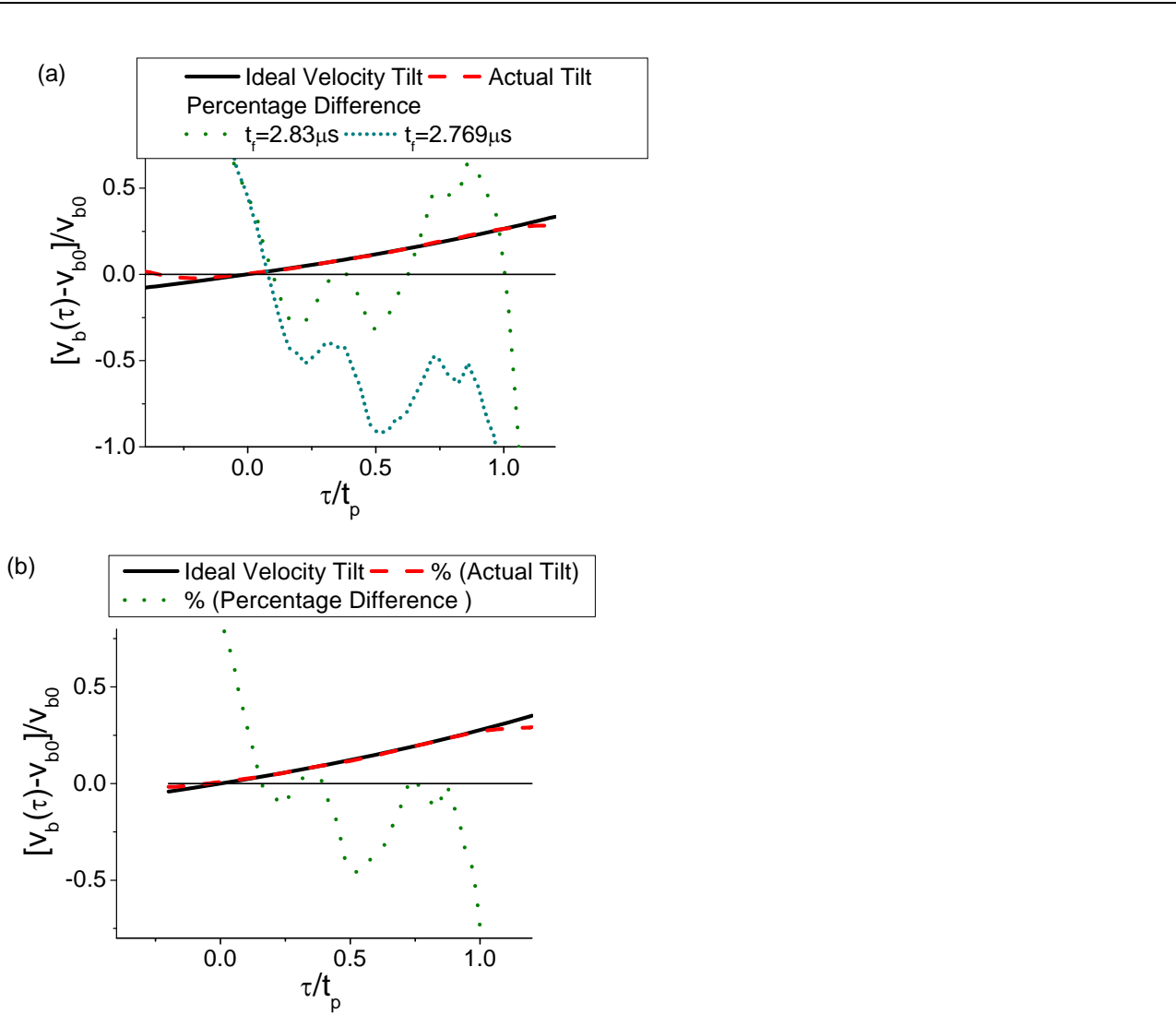


Fig. 2. The normalized beam velocity tilt $\Delta v_b / v_{b0}$ is plotted as a function of normalized time τ / t_p in the tilt core for the voltage pulse waveform shown in Fig. 1. The solid curve shows the ideal velocity tilt given by Eq. (6) for (a) $t_f = 2.83 \mu\text{s}$, $E_{b0} = 210 \text{ keV}$ and $t_f = 2.679 \mu\text{s}$, $E_{b0} = 217 \text{ keV}$, and (b) $t_f = 2.725 \mu\text{s}$, $E_{b0} = 208 \text{ keV}$. The dashed and dotted curves show the experimental velocity tilt and the value of the error in percent, respectively.

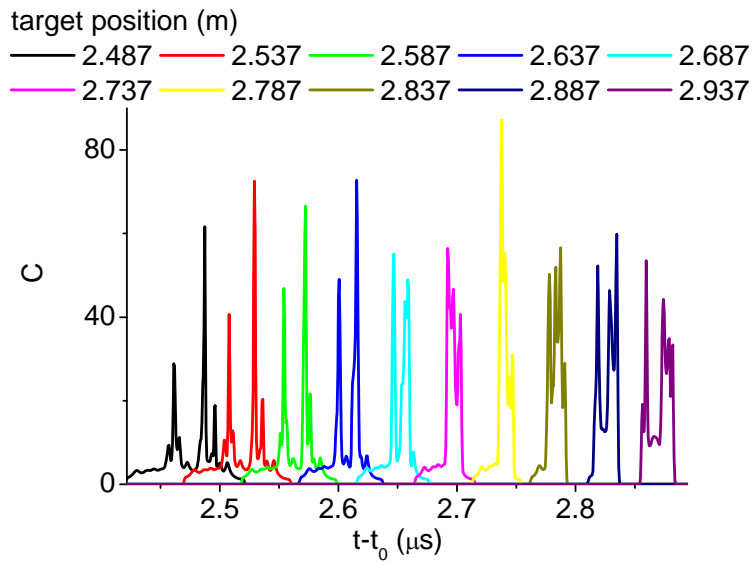
182
183

184 III.B Spread of compression locations due to fast changing errors in the voltage pulse 185

186 From Fig. 3 it is evident that the beam pulse compresses significantly at different positions, which
187 are spread over large distances relative to the target plane. This behavior can be explained by
188 plotting the times when different parts of the beam pulse compress according to Eq. (8), as shown in
189 Fig. 4. The compression time, or the time when neighboring slices of the beam arrive at the same

190 position, depends on the time derivative of the voltage waveform. Therefore, small but fast-
 191 changing errors result in large variations of the compression time of different parts of the beam
 192 pulse. That is, one percent errors in the beam velocity tilt can result in 10 to 20 percent variations of
 193 the compression time, as evident from Fig. 4. A zoomed-in plot of the compression ratio is shown
 194 in Fig. 5. It is evident from Fig. 5 that the compressed pulse foot width is of order 10ns due to the
 195 errors, but the compressed pulse full width at half maximum can be reduced to a few ns for
 196 optimum beam energy [compare Fig. 5 (a) and (b)]. Indeed, if there is an error in the beam velocity,
 197 δv_b , due to voltage errors, the beam pulse width at the target plane is $\delta v_b t_f$.

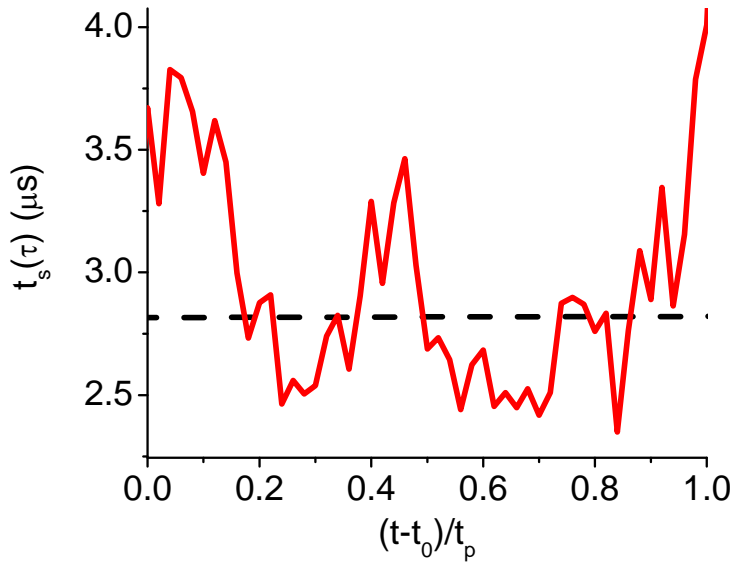
198



199

200 Fig. 3. Simulated compressed pulse waveform at ten different target locations from $z=248.7$ cm to 293.7 cm plotted as a
 201 function of drift time after the beam pulse passes through the induction bunching module for the voltage waveform
 202 shown in Fig. 1. The beam energy is 270 keV, and the longitudinal temperature, T_z , is 0.05 eV.

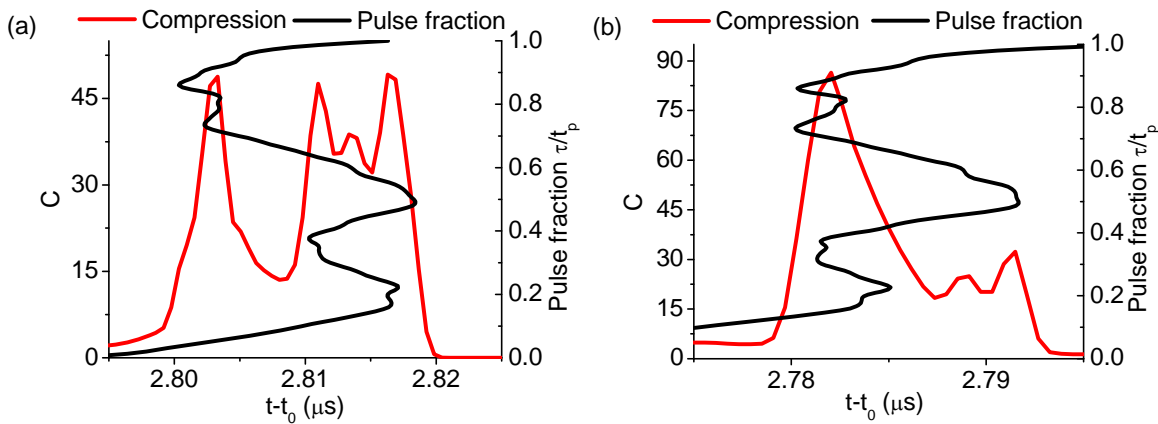
203



204

205 Fig. 4. The time $t_s(\tau)$, when neighboring slices of the beam arrive at the same position, is plotted as a function of
 206 normalized time, $(t - t_0) / t_p$, where $\tau = t - t_0$. The solid (red) curve corresponds to the experimental voltage
 207 waveform shown in Fig. 1, and the dashed (black) curve corresponds to the ideal voltage pulse.

208

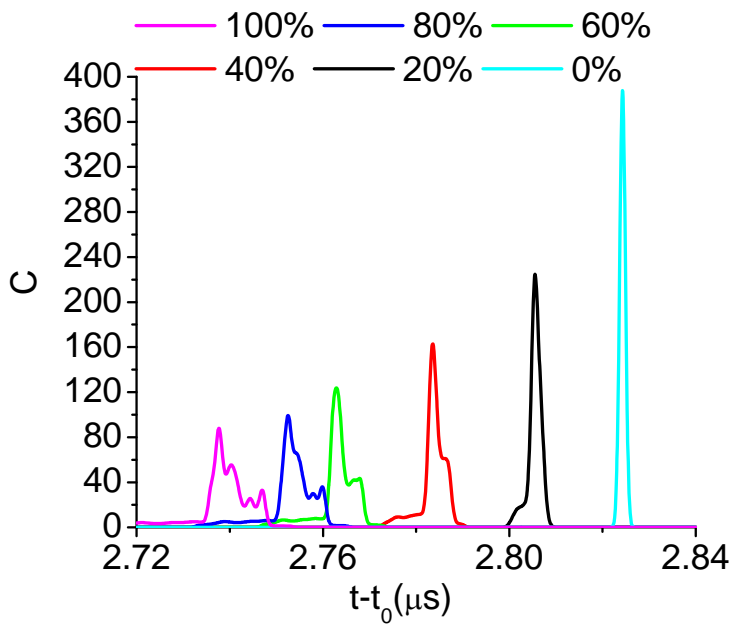


209

210 Fig. 5. The simulated compressed pulse waveform at the target location $z=286.8$ cm is plotted as a function of the drift
 211 time for the voltage waveform shown in Fig. 1. The beam energy is (a) 270keV and (b) 276keV, and the longitudinal
 212 temperature is $T_z=0.05$ eV.

213

214



215

216 Fig. 6. Simulated compressed pulse waveform at optimal target locations (100% error $z=279\text{cm}$; 80%, 280cm; 60%,
 217 281cm; 40%, 284cm; 20%, 286cm; 0%, 288cm) is plotted for reduced voltage errors as a function of drift time for the
 218 voltage waveform shown in Fig. 1. The beam energy is 270keV, and the longitudinal temperature is $T_z=0.05\text{eV}$.

219

220

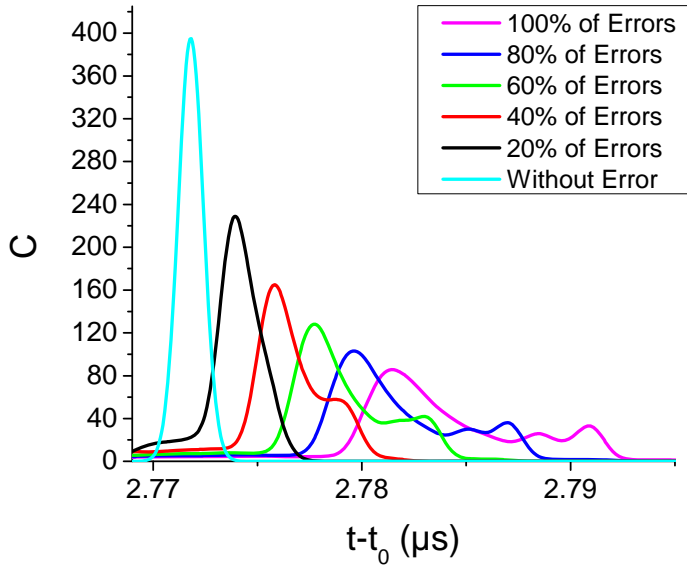
221 Correspondingly, the beam pulse duration at the target plane due to voltage errors of 1kV for a
 222 300keV beam is $\delta v_b t_f / v_{b0} \sim 2.8\mu\text{s} / 300 \approx 10\text{ns}$. For the optimum beam energy or target
 223 location, the voltage errors are a factor of three smaller for this part of the beam pulse (see Fig. 2),
 224 and the corresponding compressed pulse width is reduced from 10ns to 3ns [compare Fig. 5 (a) and
 225 Fig. 5 (b) or Fig. 3, for $z_t=2.737\text{m}$ and $z_t=2.787\text{m}$].

226

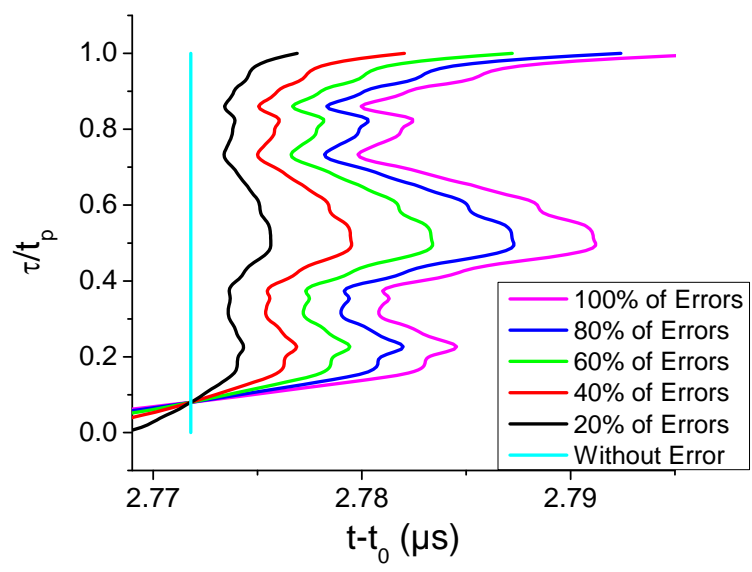
227 *III.C Scaling of the compression ratio with reduced voltage errors*

228

229 If the voltage errors are reduced, the compressed beam pulse width is also reduced and the
 230 compression ratio is increased. The effect of reduced errors is shown in Fig. 6 and Fig. 7. Reducing
 231 the errors by a factor of five only increases the compression ratio by a factor of two (compare black
 232 and magenta curves in Fig. 6 and Fig. 7). This is in agreement with Eq. (11), which shows that the
 233 compression ratio is inversely proportional to the square root of the velocity errors and the thermal
 234 spread, as shown in Fig. 8.



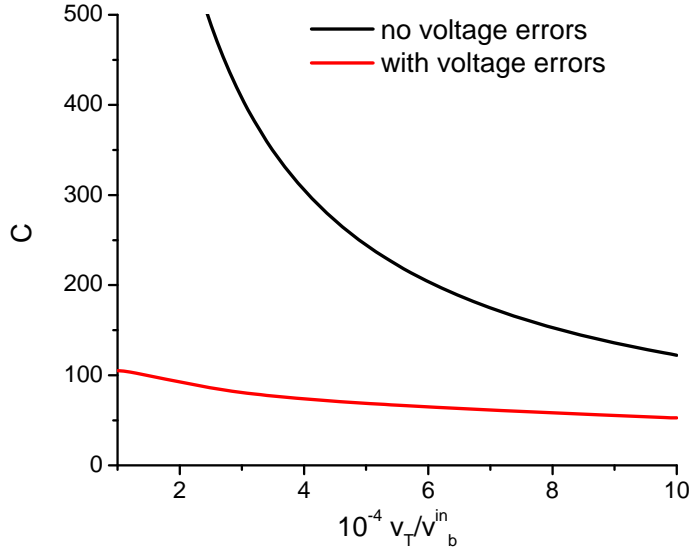
235



236

237 Fig. 7. Simulated compressed pulse waveform (top) and original pulse Lagrangian coordinate τ (bottom) at the target
 238 location, $z=286.8$, for reduced voltage errors are plotted as a function of drift time for the voltage waveform shown in
 239 Fig. 1. The longitudinal temperature is $T_z=0.05\text{eV}$.

240



241

242 Fig. 8. Simulated compression ratio at the target location, $z=2.77\text{cm}$, and drift time, $t-t_0=2.73\text{ms}$, is plotted as a
 243 function of the normalized thermal velocity, v_T / v_b^{in} , for the voltage waveform shown in Fig. 1. The beam energy is
 244 270keV , and the longitudinal temperature, $T_z=0.05\text{eV}$, corresponds to $v_T / v_b^{in} = 3 \times 10^{-4}$. The black curve
 245 corresponds to the ideal velocity tilt with no errors, and the compression ratio as a function of the thermal spread is
 246 given by Eq. (10).

247

248 *III.D Observation of multiple peaks and optimization of compressed beam pulse by varying the*
 249 *beam energy*

250

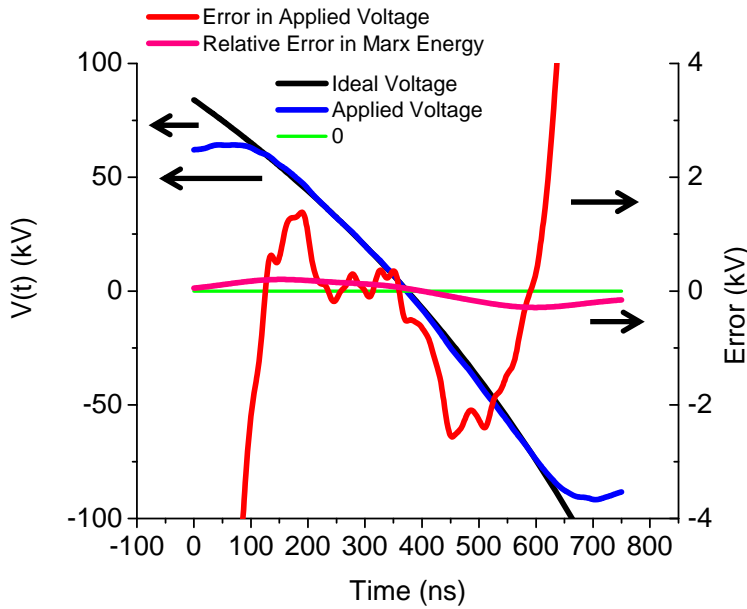
251 If the voltage profile is smooth, the beam compresses at an optimal location, and then two peaks
 252 appear, corresponding to compression in the head and tail [see Ref. [5]]. This is similar to
 253 compression in klystrons, however, in the induction bunching module with many separate pulsed
 254 elements, the fast-changing voltage errors lead to the formation of multiple peaks. The optimal
 255 compression corresponds to the case when a few major peaks overlap, or equivalently, when
 256 voltage errors are minimized for a few portions of the beam pulse. We demonstrate this by
 257 analyzing the compression with an improved voltage pulse on NDCX-I compared to the one shown
 258 in Fig. 1.

259

260 NDCX-I improvements in the induction bunching module reduced voltage errors; however, the
 261 errors are still of order $\sim 1\text{keV}$. There is a portion of the pulse near the middle where the errors are
 262 low, and this allows more of the pulse to compress at the focusing time, thereby increasing the

263 compression ratio and reducing the pulse length. This can be compared with the middle of the
 264 previous waveform, which did not compress with the rest of the beam pulse, leaving a significant
 265 portion of the pulse uncompressed.

266
 267
 268



269

270 Fig. 9. Plots of improved experimental voltage waveform of the NDCX-I induction bunching module as a function of
 271 time, and the ideal voltage waveform needed to compress the beam pulse at the target plane for beam energy 319keV
 272 (black curve). Also shown is the Gaussian-weighted averaged value of the error (with a 21ns time window) in the
 273 experimental voltage as compared with the ideal voltage pulse. Finally, the relative error in beam energy delivered by
 274 the Marx generator is shown to be small compared with applied voltage error.

275

276

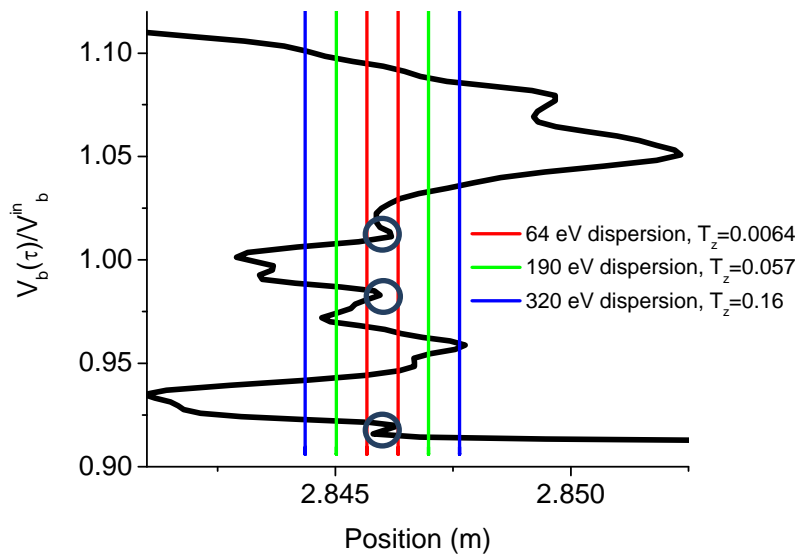
277 The thermal spread length is the mean drift length of the ions due to the intrinsic thermal energy
 278 spread of the beam pulse, $\pm v_T t_f$. Fig. 10 shows that much of the pulse does not compress within a
 279 distance $\pm v_T t_f$, even for the time of optimal compression. Errors need to be reduced by a factor of
 280 ten to be on the same order as the thermal energy spread, $\sim 100\text{eV}$. Figures Fig. 11 and Fig. 12 show
 281 that the pulse represented by the waveform in Fig. 9 compresses for a wide range of locations near
 282 the target plane. The time to focus, t_s , in Fig. 11 can be compared to the drift time, $t - t_0$, in Fig.

283 12.

284

285

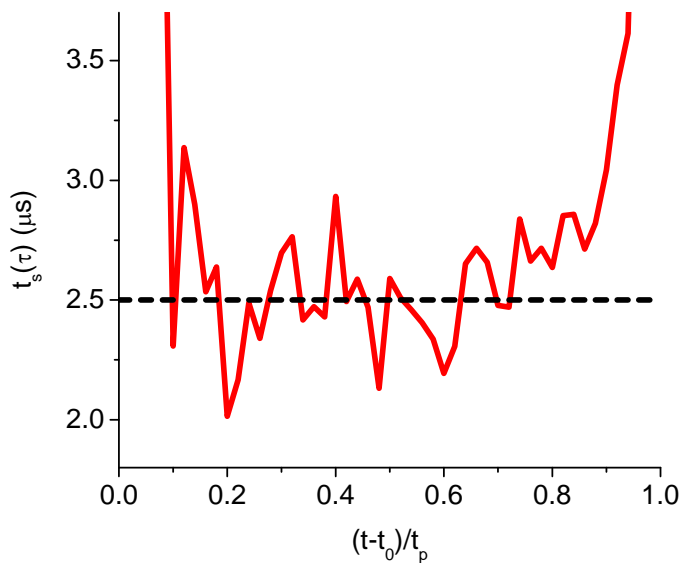
286



287

288 Fig. 10. Phase space plot of the pulse with different mean thermal energy spreads, $E_{b0} = 322\text{keV}$ and $t_f = 2.628$. The
289 target location is 2.846m. The parallel red lines indicate a mean particle drift due to a thermal energy spread of 64eV;
290 the parallel green lines correspond to a spread of 190eV; and the parallel blue lines correspond to 320eV. The three
291 circles represent regions of high density.

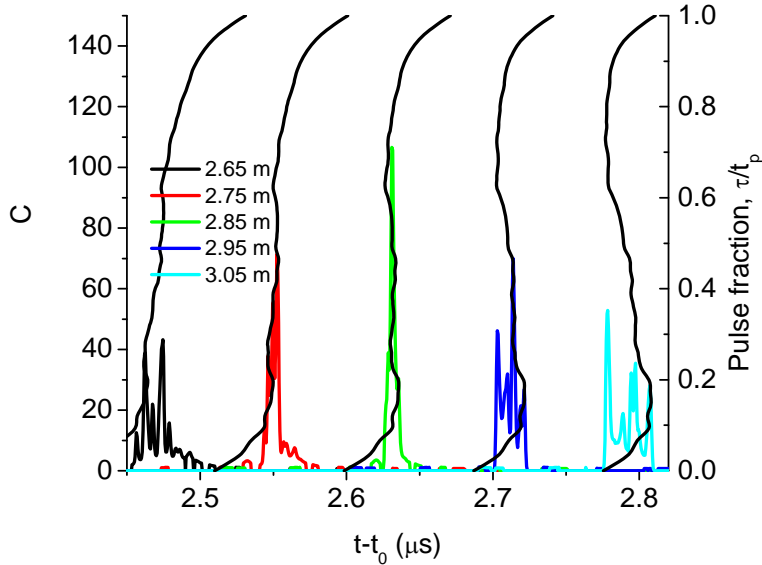
292



293

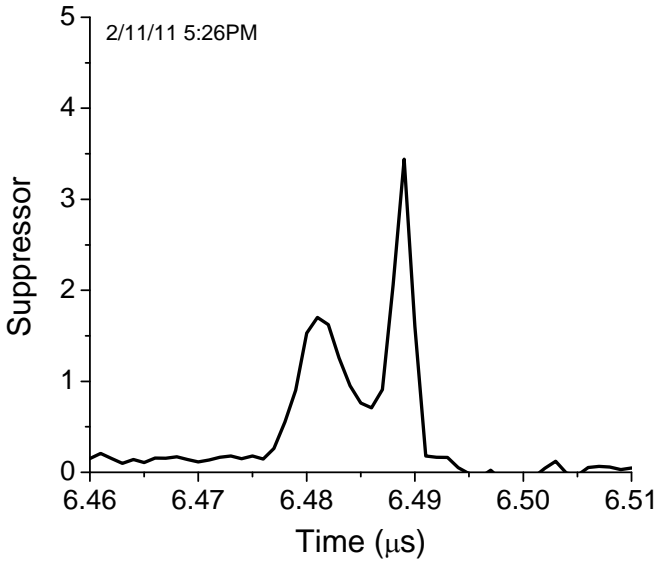
294

295 Fig. 11. The time $t_s(\tau)$, when neighboring slices of the beam arrive at the same position, is plotted as a function of
 296 normalized time $(t - t_0) / t_p$, where $\tau = t - t_0$. The solid (red) curve corresponds to the experimental voltage
 297 waveform shown in Fig. 9, and the dashed (black) curve corresponds to the ideal voltage pulse.
 298
 299



300
 301 Fig. 12. Simulated compressed pulse waveform at five different target locations, from $z=265\text{cm}$ to 305cm , plotted as a
 302 function of drift time after the beam pulse passes through the induction bunching module for the voltage waveform
 303 shown in Fig. 9. The beam energy is 322keV , the energy spread, ΔE_b , is 190eV , and $T_z=0.057\text{eV}$.

304
 305 The compression ratio profile in NDCX-I is measured using a Fast Faraday Cup (FFC), which has a
 306 time-scale response of 1ns [13]. During the initial tuning process of the experiment, multiple peaks
 307 are often observed before the final calibrations are made, as shown in Fig. 13. The energy of the
 308 beam, E_{b0} , needs to be tuned to ensure that the beam focuses at the target plane. However,
 309 compression is still observed even before the final tuning, indicating that the beam compresses over
 310 a range of target locations.



311

312

313 Fig. 13. Ion beam compression ratio profile in a pre-tuned shot from NDCX-I, as measured by a Fast Faraday Cup.

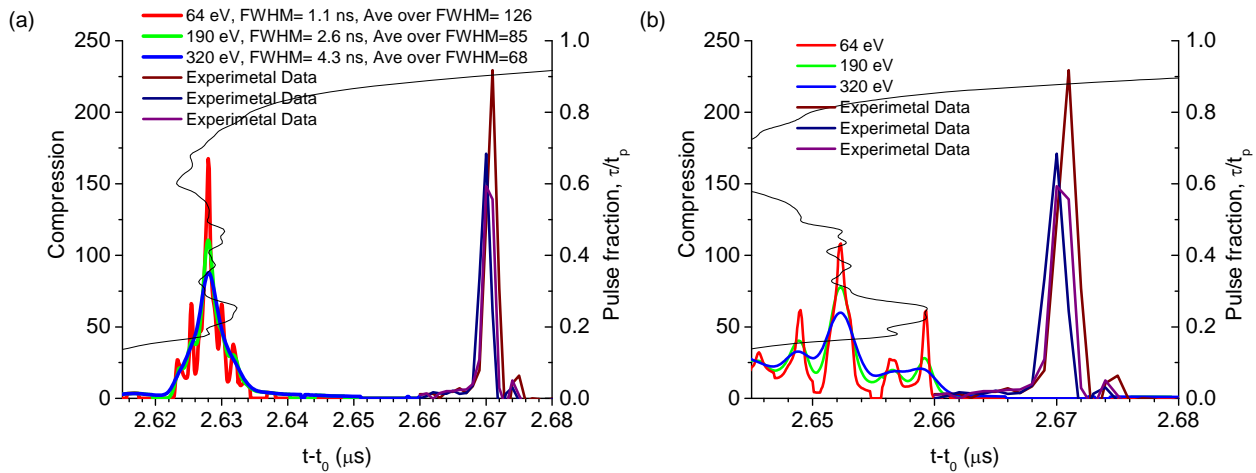
314

315 Fig. 14 compares simulated results with the results of the experiment. Fig. 14 (a) compares the
 316 optimal compression ratio obtained from the analytical formulas with the optimal experimental
 317 results. Fig. 14 (b) compares the optimal results from the experiment and the analytical formulas
 318 with the parameters, beam energy and target location, which were used in the experiment. The
 319 optimal results from the experiment more closely resemble the optimal results from the simulations.
 320 This is because the experiment is finely tuned in order to achieve the best results. To accurately
 321 analyze the data, the simulated beam energies were slightly varied to achieve the best results.

322

323

324



325

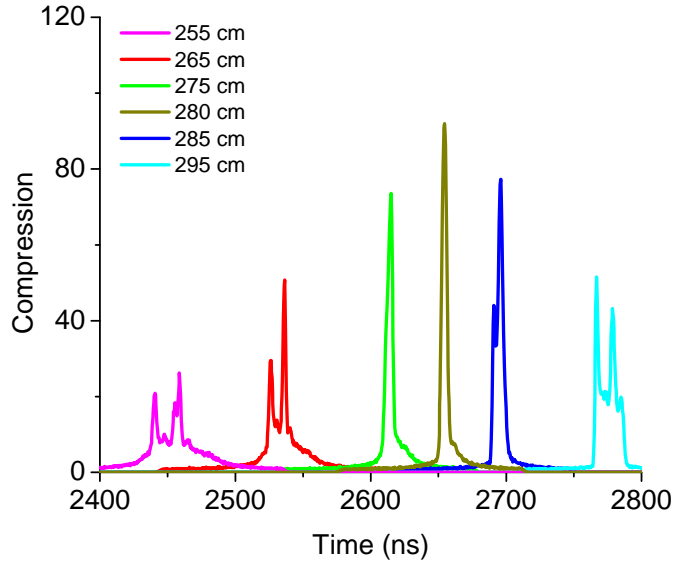
326 Fig. 14. Optimization of the simulated compressed pulse waveform for two beam energies at $z=2.846\text{m}$, (a) $E_{b0} =$
 327 316keV and (b) $E_{b0} = 322\text{keV}$, as a function of drift time, $t-t_0$, after the beam pulse passes through the induction
 328 bunching module for the voltage waveform shown in Fig. 9. This is shown together with the results for three different
 329 experimental shots.

330

331 The results have also been simulated with the LSP particle-in-cell code [9] and showed good
 332 agreement with simulated compression ratio profiles obtained from the analytical formula in Eq.(9)
 333 (performed in Mathcad). The results of both simulations are identical, granted that both codes
 334 provide adequate resolution. As was observed with the Mathcad simulations, the results from the
 335 LSP PIC code simulations show that different parts of the beam compress over a wide range of
 336 target locations, as shown in Fig. 15. Fig. 16 compares the peak compression ratio profile obtained
 337 from the LSP simulations with the experimental results shown above. Fig. 17 compares the same
 338 LSP results with the peak compression ratio profile simulated by Mathcad using the same input
 339 parameters.

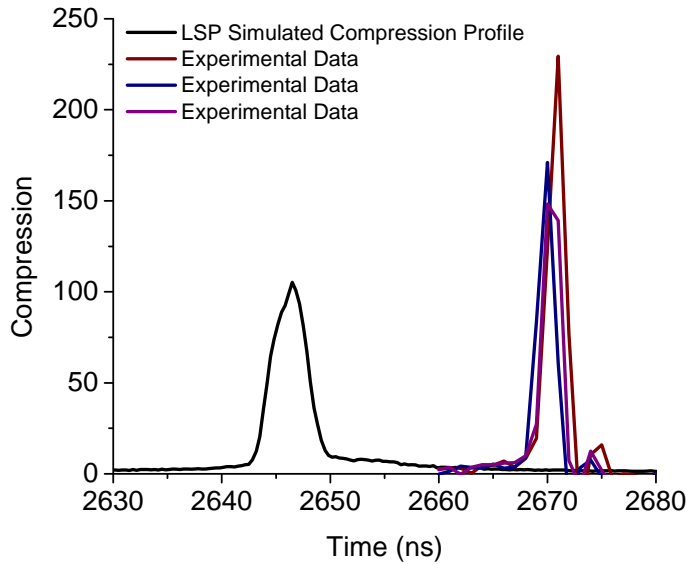
340

341



342

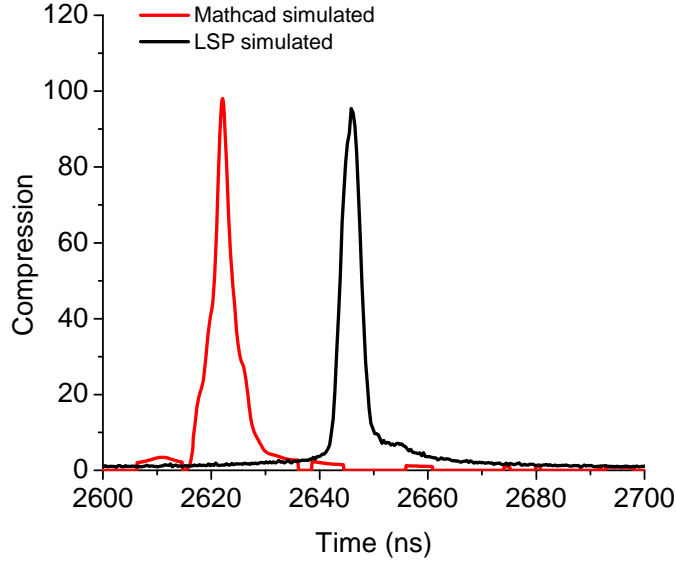
343 Fig. 15. Simulated compressed pulse waveform at six different target locations, from $z=255$ cm to 295 cm as a function
 344 of drift time after the beam pulse passes through the induction bunching module for the voltage waveform shown in
 345 Fig. 9. The beam energy is 317keV, and the energy spread, ΔE_b , is 252eV, where $T_{bz}=0.1$ eV.



346

347 Fig. 16. LSP-simulated compression ratio profile compared with experimental results. For the LSP simulations,
 348 $z=2.79$ m, and $E_{b0}=317$ keV. The energy spread, ΔE_b , is 252eV, corresponding to $T_{bz}=0.05$ eV.

349



350

351 Fig. 17. Comparison of LSP simulations with Mathcad simulations. For Mathcad, $z=2.77\text{m}$. For LSP, $z=2.79\text{m}$. $E_{b0} =$
 352 317keV . The energy spread, ΔE_b , is 252eV , or $T_{bz}=0.1\text{eV}$. The small difference in the focusing time, t_f , is associated
 353 with the finite gap effects of the NDCX-I induction bunching module [5]. This has the effect of shifting the applied
 354 velocity tilt profile to be slower than that estimated using the thin gap approximation.

355

356 IV. CONCLUSIONS

357

358 In this paper the NDCX-I experimental data for longitudinal compression of the beam pulse has
 359 been analyzed. A typical voltage pulse produced in the bunching module of NDCX-I was shown in
 360 Fig. 1, along with the voltage errors. A voltage pulse in the bunching module with amplitude of
 361 $\Delta U \approx 100\text{kV}$ results in the beam pulse compressing from $t_p = 590\text{ns}$ down to $\delta t_p \approx 3.2\text{ns}$ during
 362 $t_f = 2.8\mu\text{s}$ of the neutralized drift over 2.68m . The voltage error, δU , is in the kV range. The errors
 363 in the applied voltage are much larger than the thermal energy spread, which is of order 100eV , and
 364 they dominate the compression process.

365

366 For a 300keV beam in NDCX-I, the spread in arrival time for the entire beam pulse at the target
 367 plane due to voltage errors and corresponding errors in the beam velocity, δv_b , is

368
$$\delta t_p = t_f \delta v_b / v_{b0} = t_f \delta U / E_{b0} \sim 2.8\mu\text{s} / 300 \approx 10\text{ns}.$$
 However, at certain locations, a fraction of

369 the beam is compressed more tightly if the voltage errors for this portion of the beam pulse are

370 minimized. For example, for NDCX-I parameters, it was shown that the half-width of the
371 compressed beam pulse can be reduced from 10ns to 2ns.

372

373 Improvements in NDCX-I voltage waveform reduce the voltage errors and allow a larger fraction of
374 the beam pulse to compress, thereby increasing the compression ratio and reducing the compressed
375 pulse width. However, because voltage errors are still large, different parts of the pulse compress
376 over a range of times, causing the pulse to be compressed for many target locations. The beam
377 energy can be optimized to reduce the errors of the applied voltage waveform and obtain one single
378 peak at the target. This corresponds to the case when the applied voltage waveform can be
379 approximated by an ideal voltage curve that compresses at the target plane with smaller voltage
380 errors for a larger fraction of the beam pulse.

381

382 **ACKNOWLEDGEMENTS**

383

384 Research performed under the auspices of the U.S. Department of Energy by the Princeton Plasma
385 Physics Laboratory under Contract DE-AC02-76CH03073 and Lawrence Livermore National
386 Laboratory under Contract DE-AC52-07NA27344.

387

388 **REFERENCES**

-
- [1] P. Sing Babu, A. Goswami, V.S. Pandit, Nucl. Instr. and Meth. Phys. Res. A **642**, (2011) 1; A. V. Eliseev, I. N. Meshkov, V. A. Mikhailov and A. O. Sidorin, Physics of Particles and Nuclei Letters 7, (2010) 473; T. Kikuchi, K. Horioka, M. Nakajima, S. Kawata, Nucl. Instr. and Meth. Phys. Res. A 577, (2007) 103; G. Franchetti, I. Hofmann, and G. Rumolo, Phys. Rev. ST Accel. Beams 3, (2000) 084201; J.G. Wang, D.X. Wang, M. Reiser, Nucl. Instr. and Meth. Phys. Res. A 316, (1992) 112; S. Humphries, Journal of Applied Physics 51, (1980) 2338.
- [2] D.R. Welch, et al., Nucl. Instr. and Meth. Phys. Res. A **544**, (2005) 236.
- [3] P.K. Roy, et al., Nucl. Instr. and Meth. Phys. Res. A **606**, (2009) 22.
- [4] R.C. Davidson, et al., Phys. Rev. Special Topics – Accelerators and Beams Vol. **7**, (2004) 104201.

-
- [5] I. D. Kaganovich, et al., “Effects of Errors in Velocity Tilt on Maximum Longitudinal Compression During Neutralized Drift Compression of Intense Beam Pulses: I. General Descriptions.”
- [6] J.E. Coleman, et al., in Proceedings of the Particle Accelerator Conference, Albuquerque, NM, June25–29 (IEEE catalog #07 CH37866, USA, 2007),
[/http://accelconf.web.cern.ch/accelconf/p07/PAPERS/THPAS004.PDFS](http://accelconf.web.cern.ch/accelconf/p07/PAPERS/THPAS004.PDFS), 2007, pp. 3516–3518; J.E. Coleman, Intense ion beams for warm dense matter physics, Ph.D. Thesis, University of California, Berkeley, 2008.
- [7] J.E. Coleman, et al., in Proceedings of the Particle Accelerator Conference, Albuquerque, NM, June25–29 (IEEE catalog #07 CH37866, USA, 2007),
[/http://accelconf.web.cern.ch/accelconf/p07/PAPERS/THPAS004.PDFS](http://accelconf.web.cern.ch/accelconf/p07/PAPERS/THPAS004.PDFS), 2007, pp. 3516–3518; J.E. Coleman, Intense ion beams for warm dense matter physics, Ph.D. Thesis, University of California, Berkeley, 2008.
- [8] P. K. Roy et al., Nucl. Instr. and Meth. in Phys. Res. A **577**, (2007) 223; P.K. Roy *et al.*, Phys. Rev. ST Accel. Beams **9**, (2006) 070402.
- [9] A. B. Sefkow et al., Phys. Plasmas **16**, (2009) 056701; A. B. Sefkow and R. C. Davidson, Physical Review Special Topics on Accelerators and Beams **10**, (2007) 100101; A. B. Sefkow, Ph.D. Thesis, Princeton University (2007).
- [10] P. Seidl *et al.*, Proceedings of the 2009 Particle Accelerator Conference, Vancouver, BC, Canada, TH3GAI04 <http://trshare.triumf.ca/~pac09proc/Proceedings/papers/th3gai04.pdf> ; P.K. Roy *et al.*, Phys. Rev. Lett. **95**, (2005) 234801
- [11] J.E. Coleman, et al., in Proceedings of the Particle Accelerator Conference, Albuquerque, NM, June25–29 (IEEE catalog #07 CH37866, USA, 2007),
[/http://accelconf.web.cern.ch/accelconf/p07/PAPERS/THPAS004.PDFS](http://accelconf.web.cern.ch/accelconf/p07/PAPERS/THPAS004.PDFS), 2007, pp. 3516–3518; J.E. Coleman, Intense ion beams for warm dense matter physics, Ph.D. Thesis, University of California, Berkeley, 2008.
- [12] P. A. Seidl, A. Anders, F. M. Bieniosek, J. J. Barnard, J. Calanog, A.X. Chen, R.H. Cohen, J. E. Coleman, M. Dorf, E. P. Gilson, D.P. Grote, J.Y. Jung, M. Leitner, S. M. Lidia, B. G. Logan, P. Ni, P. K. Roy, K. Van den Bogert, W.L. Waldron, D.R. Welch, Nucl. Instr. and Meth. Phys. Res. A **606**, (2009) 75–82.

[13]S. M. Lidia, P.K. Roy, P.A. Seidl, W.L. Waldron, E.P. Gilson, “Commissioning results of the upgraded neutralized drift compression experiment” in 2009 Proceedings of the Particle Accelerator Conference, Vancouver, BC, Canada, TU6PFP092,
<http://trshare.triumf.ca/~pac09proc/Proceedings/papers/tu6pfp092.pdf>